

Influence of pulse duration on ultrashort laser pulse ablation of biological tissues

Beop-Min Kim

Yonsei University
Department of Biomedical Engineering
234 Maeji, Heungup
Wonjoo, Kangwon-Do, 220-710 Korea

Michael D. Feit

Alexander M. Rubenchik

Elizabeth J. Joslin

Peter M. Celliers

Jürgen Eichler

Luiz B. Da Silva

Medical Technology Program
Lawrence Livermore National Laboratory
P.O. Box 808
Livermore, California 94551

Abstract. Ablation characteristics of ultrashort laser pulses were investigated for pulse durations in the range of 130 fs–10 ps. Tissue samples used in the study were dental hard tissue (dentin) and water. We observed differences in ablation crater morphology for craters generated with pulse durations in the 130 fs–1 ps and the 5 ps–10 ps range. For the water experiment, the surface ablation and subsequent propagation of stress waves were monitored using Mach–Zehnder interferometry. For 130 fs–1 ps, energy is deposited on the surface while for longer pulses the beam penetrates into the sample. Both studies indicate that a transition occurs between 1 and 5 ps. © 2001 Society of Photo-Optical Instrumentation Engineers. [DOI: 10.1117/1.1381561]

Keywords: ultrashort laser pulse; pulse duration; ablation; biological tissues.

Paper 90065 JBO received Dec. 7, 1999; revised manuscript received Dec. 29, 2000; accepted for publication Jan. 3, 2001.

1 Introduction

Intense laser pulses can ionize atoms and break up molecules to create high temperature plasmas (ions and electrons). In plasma-mediated ablation the laser energy is absorbed by electrons which transfer their energy through collisions to the ions. The absorption coefficient of plasma is typically several orders of magnitude higher than that of the un-ionized material. The result is that laser absorption occurs in a very thin layer of material. In the case of ultrashort laser pulses (USLP) (pulse duration < 1 ps) most absorption occurs in depth less than 1000 Å. Using USLP reduces the amount of energy transfer to the deeper (unablated) layers since the plasma expands rapidly, which results in rapid cooling. Also, the amount of energy transferred from the electrons to the ions (or lattice) is reduced. These effects have been used to explain the low thermal collateral damage produced by USLP.^{1–7} The other advantage of USLP ablation is that the generated shock wave is quickly attenuated before propagating very far into the material. For nanosecond lasers the absorption process is complicated by plasma expansion which can generate an absorbing plume of low density material several hundred microns thick. In this case the region of maximum absorption is decoupled from the ablation front thereby reducing the ablation efficiency.

Numerous efforts have been made to apply USLP in medicine. Examples include dentistry,^{8–10} ophthalmology,^{11–14} and neurosurgery.¹⁵ Many of these applications take advantage of the minimal damage, high precision, and high ablation efficiency of USLP ablation.

Clinical use of subpicosecond pulses in tissue ablation is not practical at this stage. It is still too expensive to build subpicosecond lasers compared to longer pulse lasers. Also, due to group velocity dispersion and fiber damage problems, it is difficult to use standard optical fibers for USLP delivery.

This necessitates the use of an articulated arm. It is therefore of interest to compare the characteristics of ablation using subpicosecond pulses with a few picosecond pulses since it is conceivable that the few picosecond laser pulses might be transmitted through fibers with less detrimental effects of dispersion and fiber damage. It is also likely that picosecond lasers will cost less than femtosecond lasers.

The objective of this study is to investigate ablation in the low picosecond and subpicosecond range of pulse duration. For the hard tissue experiment, ablation craters were examined for the pulse duration range of 130 fs–10 ps. As a close approximation of soft tissue ablation, water ablation was studied using Mach–Zehnder interferometry. Patterns of shock wave generation in water due to USLP were investigated in the same pulse duration range. In fact, the shadowgraph method used by other researchers might give clearer pictures of the shock waves.^{16–18} However, interferometry was used so that the pressure could be quantified, which will be published in a separate report in the future.

2 Materials and Methods

The complete ultrashort pulse laser system was composed of four separate, commercially available lasers. The actively mode-locked oscillator (Spectra-Physics, Tsunami) produced an 80 MHz pulse train with maximum output power of 800 mW at 800 nm. This oscillator was pumped by a 5 W, continuous, frequency-doubled Nd:YAG laser (Spectra-Physics, Millennia). The 80 MHz pulse train was amplified in a regenerative amplifier (Positive Light, Spitfire) by the chirped-pulse amplification process. The regenerative amplifier was pumped by a Q-switched Nd:YLF laser (Positive Light, Merlin). The maximum output energy of the amplified pulse was 1 mJ/pulse at 800 nm and the pulse duration could be continuously changed by controlling the path length of the beam in the

Address all correspondence to Beop-Min Kim, E-mail: beopmkim@dragon.yonsei.ac.kr
Jürgen Eichler is also affiliated with Technische Fachhochschule-Berlin, University of Applied Science, Seestr. 64, 13347 Berlin, Germany.

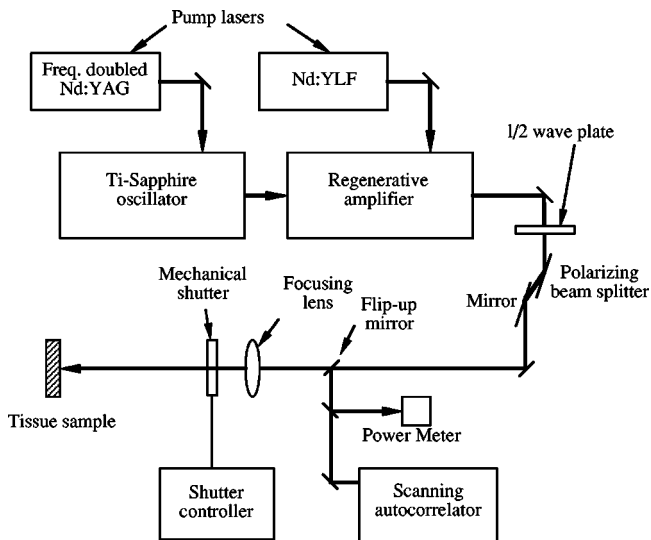


Fig. 1 Experimental setup for hard tissue ablation. The pulse energy is controlled by rotating the $\lambda/2$ wave plate. The energy per pulse and the pulse duration are measured by directing the beam to the power meter and to the autocorrelator. The mechanical shutter was used for allowing 1000 shots for each ablation craters. The repetition rate was 1 kHz and the beam size was 130 fs.

compressor. A scanning autocorrelator was used to measure the pulse duration and the shortest pulse duration was 130 fs.

The schematic of the experimental setup is shown in Figure 1. The output beam energy was controlled by rotating the zeroth-order half-wave plate placed in front of the 72° polarizing beam splitter and matching 72° mirror. Energy transmitted through the beam splitter was dumped and only the reflected beam was used for tissue ablation. The beam was focused using a 500 mm focal length antireflection-coated lens for hard tissue experiment and using a 250 mm lens for water experiment. The beam size was imaged at the focal plane using a microscope objective and a charge coupled device (CCD) camera (Cohu Inc.). The spot image was displayed using a beam analyzer (Spiricon Inc.). The focal position of the focus was found by moving the objective and CCD camera along the beam path and searching for the smallest spot size. The beam mode was close to TEM₀₀ for all cases without noticeable hot spots and the beam size was 130 μm for hard tissue studies and 60 μm for water ablation experiment.

2.1 Hard Tissue Preparation

The hard tissue samples were human tooth slices. The teeth were collected from a local dental clinic after being sterilized. The teeth were cut into thin 600 μm thick slices using a low-speed diamond saw (Buhler Inc). After being cut, the surfaces were polished using a 0.3 mil polishing paper. The quality of the tooth slices were examined under an optical microscope, and tested for surface defects. These slices were placed on transparent glass slides and irradiated with normally incident beams. After irradiation, the dentin slices were coated with platinum–gold coating with thickness of 20 nm before seen under scanning electron microscope.

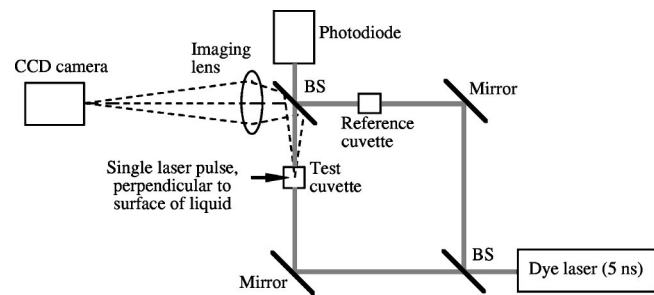


Fig. 2 Mach-Zehnder interferometer for shock wave measurement due to USLP irradiation. The photodiode signal was used to control the time delay between USLP irradiation and probe beam. The USLP is incident vertically to the water surface inside the cuvette.

2.2 Water Experiment

The USLP generated shock waves were monitored by using Mach-Zehnder interferometry. The experimental setup is shown in Figure 2. The probe beam is split into two paths using a 50/50 beam splitter. One of the beam paths contains a cuvette filled with purified water. Another water-filled cuvette is placed on the other path of the interferometer to equalize the two beam paths. The two beams were recombined in another beam splitter to generate fringe patterns. As a probe, pulses from a N_2 laser-pumped dye laser (LSI Inc) with wavelength of 480 nm and pulse duration of 4–5 ns were used. Therefore, the temporal resolution of the interferograms is 4–5 ns. The USLP was incident normal to the water surface of one of the cuvettes. The stress wave generated from the surface causes water density changes that result in the fringe shifts on the interferograms. A 50 mm camera objective (Konica Inc.) was used to image the deposition zone onto a CCD camera (Princeton Instruments Inc.). The time interval between intense USLP irradiation and probing time was controlled by triggering the ultrashort pulse laser and dye laser from a pulse generator (Stanford Inc.).

3 Results

3.1 Hard Tissue Studies

Several groups have reported the ablation thresholds of various dielectrics for multiple pulse durations.^{2,3,19} Similar measurements were performed using human dentin and the results are shown in Figure 3. For each pulse duration, the dentin slices were irradiated with 1000 pulses on a single spot and multiple spots were irradiated using a range of fluences. The ablation threshold was defined as the minimum fluence that induces morphologic changes on the dentin surface. The repetition rate was fixed at 1 kHz and the beam size was 130 μm full width half maximum. The pulse length range scanned was 130 fs–20 ps.

It is well known that the ablation thresholds for dielectrics increase as the square root of pulse duration for pulses longer than tens of picoseconds.² The threshold for dentin was found to follow the same rule for pulse durations of 5 ps and longer. The threshold scaling differs from $\tau^{1/2}$ when the pulse duration is shorter than 5 ps. Our threshold values are in agreement with published data.⁵ The threshold fluence for 130 fs was 0.75 J/cm² and increases up to 3.8 J/cm² for 20 ps which is approximately four times the 130 fs threshold. Three

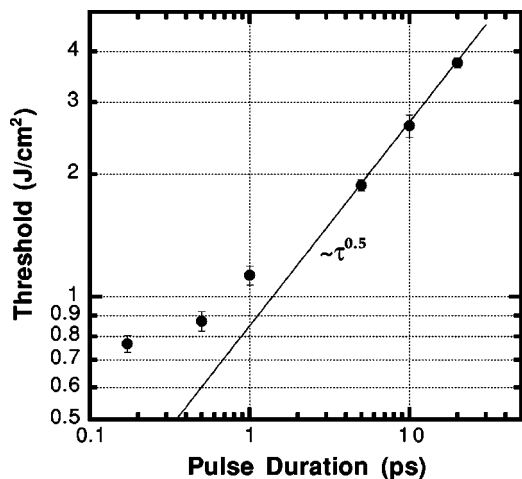


Fig. 3 Ablation threshold for human dental tissue (dentin). The minimal fluence that causes surface modification is defined as an ablation threshold for each pulse duration setting. Error bars correspond to the standard deviation from three measurement on three different tissue samples. The solid line is fitted to the data and the slope is proportional to (pulse duration)^{0.5}. The repetition rate was 1 kHz and the beam size was 130 μm.

samples were measured and the error bars correspond to the standard deviation of these three measurements.

Ablation craters were created on the dentin surface using fluences at twice the threshold values for 130 fs, 1 ps, 5 ps, and 10 ps pulses. The beam size was 130 μm for all cases. Top and side views of the craters are shown in Figure 4. These pictures were taken using scanning electron microscopy (SEM). The walls and edges of the craters created using pulse durations 1 ps and shorter show comparatively smooth surfaces. The dentin tubules are mostly intact and open, both at the wall and at the periphery of the craters. On the other hand, the pictures of craters created by 5 and 10 ps pulses show rough surfaces and melted edges.

Figure 5 shows the measured depth of the ablation craters as a function of the number of shots for 130 fs, 1 ps, and 10 ps pulses. The fluences were the same as those used for craters in Figure 4—twice the threshold values for each pulse duration. Single datum was collected for each combination of pulse duration and number of pulses. Some graphs show slightly decreased ablation depth even with increased number of shots. This is simply because of the site to site variation of different spots on the dentin. The depth of the craters could not be measured using conventional optical microscopy because it was difficult to image the bottom of the craters due to the high aspect ratio of the crater shape.²⁰ Instead, a SEM was used to measure the depth of the craters. They were measured by focusing the SEM images at the surface and at the bottom of each crater. The distance between these two foci corresponds to the crater depth. For all pulse durations a limited crater depth was achieved in a finite number of shots. This is a well-known phenomenon, and is due to the strong scaling of the ablation threshold with intensity combined with the Gaussian focal spot intensity distribution.^{10,20} From Figure 5, it is evident that the final crater depth improves with longer pulse duration. This may be caused by additional thermal ablation that is associated with longer pulse irradiation, as evi-

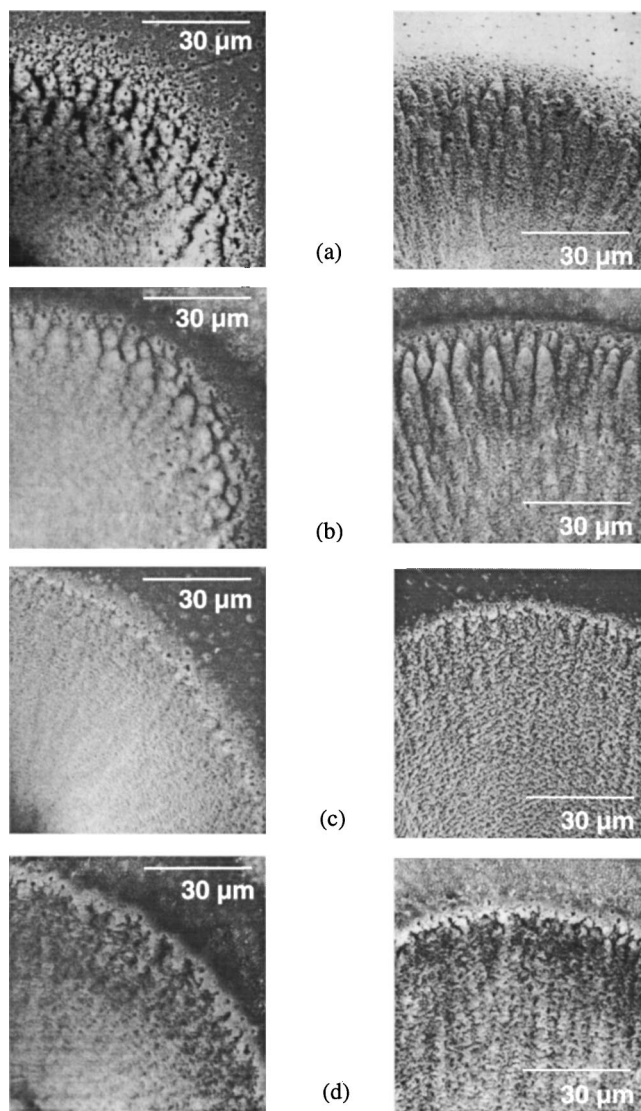


Fig. 4 Top and side view of the ablation craters created by (a) 130 fs, (b) 1 ps, (c) 5 ps, and (d) 10 ps pulses. Two times the ablation threshold values (Figure 3) were used for each crater. It is observed that the edges of 5 and 10 ps craters melted indicating thermal accumulation. For 130 fs and 1 ps craters, the dentin tubules are open and intact both at wall and edge.

denced by melting at the crater walls and edges. A detailed explanation will be given in the discussion. Figure 6 shows how the ablation efficiency (μm/μJ) drops off quickly as the number of shots increases. The initial efficiency is the highest when 130 fs is used. The ablation efficiency drops by 35% for 1 ps and by 60% for 10 ps.

3.2 Water Studies

The water ablation threshold was defined as the fluence that creates an observable spherical acoustic wave. The spherical waves are generated when the pulse energy is deposited on the surface. Figure 7 shows the measured threshold of water in the pulse duration range of 130 fs–10 ps. Similar to Figure 3, the ablation threshold scales with the square root of pulse

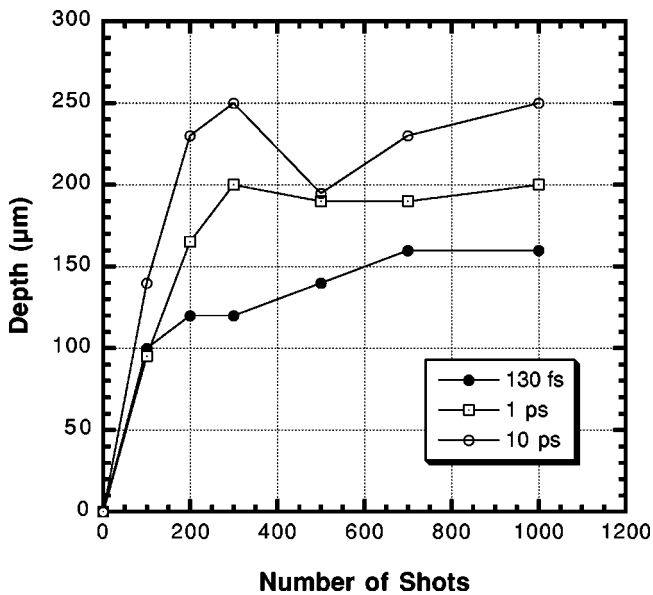


Fig. 5 Ablation depth as a function of number of USLP. Initial ablation rate is approximately $1 \mu\text{m}/\text{pulse}$ for all cases. Longer pulse duration results in moderate improvement of final depth. Variations in ablation depth after 100–200 shots are mostly due to artifacts due to inhomogeneous materials.

duration for 5 and 10 ps pulses but a reduced scaling is obtained for 1 ps and shorter pulses. The beam size was $60 \mu\text{m}$ for all cases.

Interferograms were taken near threshold using a CCD camera; resulting images are shown in Figure 8. Since the fluence is near threshold, the stress waves are barely seen in these pictures. The delay time between the USLP and probe beam was approximately 70–100 ns for all cases. The pictures for 130 fs, 500 fs, and 1 ps show a similar pattern, that is,

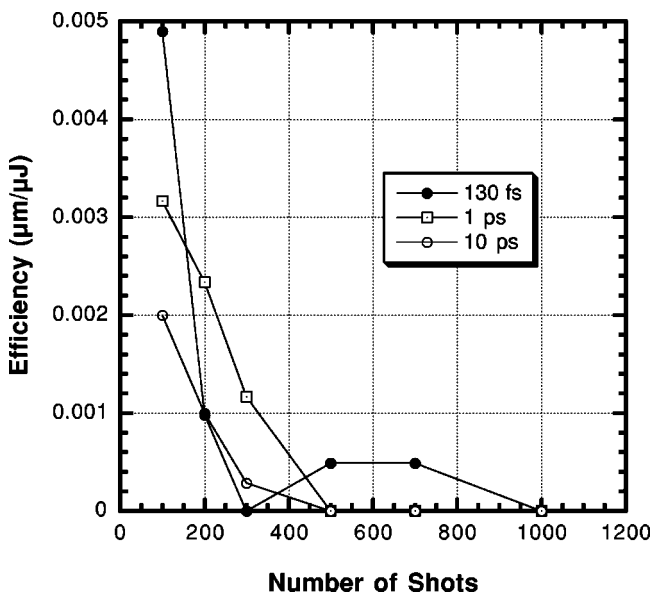


Fig. 6 Ablation efficiency defined by $\mu\text{m}/\mu\text{J}$ is the highest for 130 fs pulses and decreases with longer pulse duration. Efficiency rapidly drops to near zero after several hundred shots.

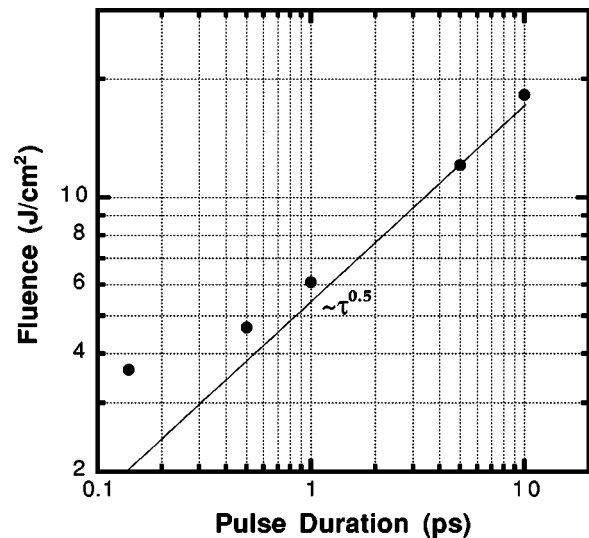


Fig. 7 Threshold fluence of water shock wave. The minimal fluence that causes surface-generated spherical shocks are defined as threshold. The solid line is fitted to the data and the slope is proportional to (pulse duration) $^{0.5}$.

stress waves were generated from the surface and propagated spherically forming hemispheres. For the cases of 5 and 10 ps, cylindrical waves propagated radially from channel formed at the beam axis in addition to the spherical waves. A transition between 1 and 5 ps pulse lengths is observed in terms of stress wave propagation. A possible explanation of this observation is presented in the latter part of this paper.

4 Discussion

Advantages of plasma-mediated ablation due to subpicosecond laser pulses have been studied theoretically and experimentally, and reported by many researchers. However, practical use of femtosecond lasers might be hindered by their high cost and difficulty in providing a delivery system. We assumed that if laser pulses in the range of 1–10 ps showed similar ablation characteristics as femtosecond pulses, the cost and delivery problems might be alleviated. This was the major issue explored in the present study.

The ablation threshold for hard dental tissue between 130 fs and 1 ps differs only by 50%, and the longer pulse offers a larger (25%) final depth. Also morphology of ablation craters formed by 130 fs and 1 ps pulses are not noticeably different. However, ablation craters formed by 5 ps and longer pulses showed more thermal damage both at the edge and wall. A larger fraction of absorbed energy of the 5 ps or longer pulses is used for heating the material rather than for material removal, which results in reduced ablation efficiency with longer pulses (Figure 6).

Considering that 70%–80% of the body mass is water, water ablation is a good approximation for soft tissue ablation except that there might be more linear absorption for biological tissues. Considering that linear absorption does not play a significant role for USP plasma-mediated ablation, this approximation is further justified. The stress waves generated with 130 fs–1 ps and 5–10 ps show clearly different patterns. For 130 fs–1 ps, only spherical waves are generated from the

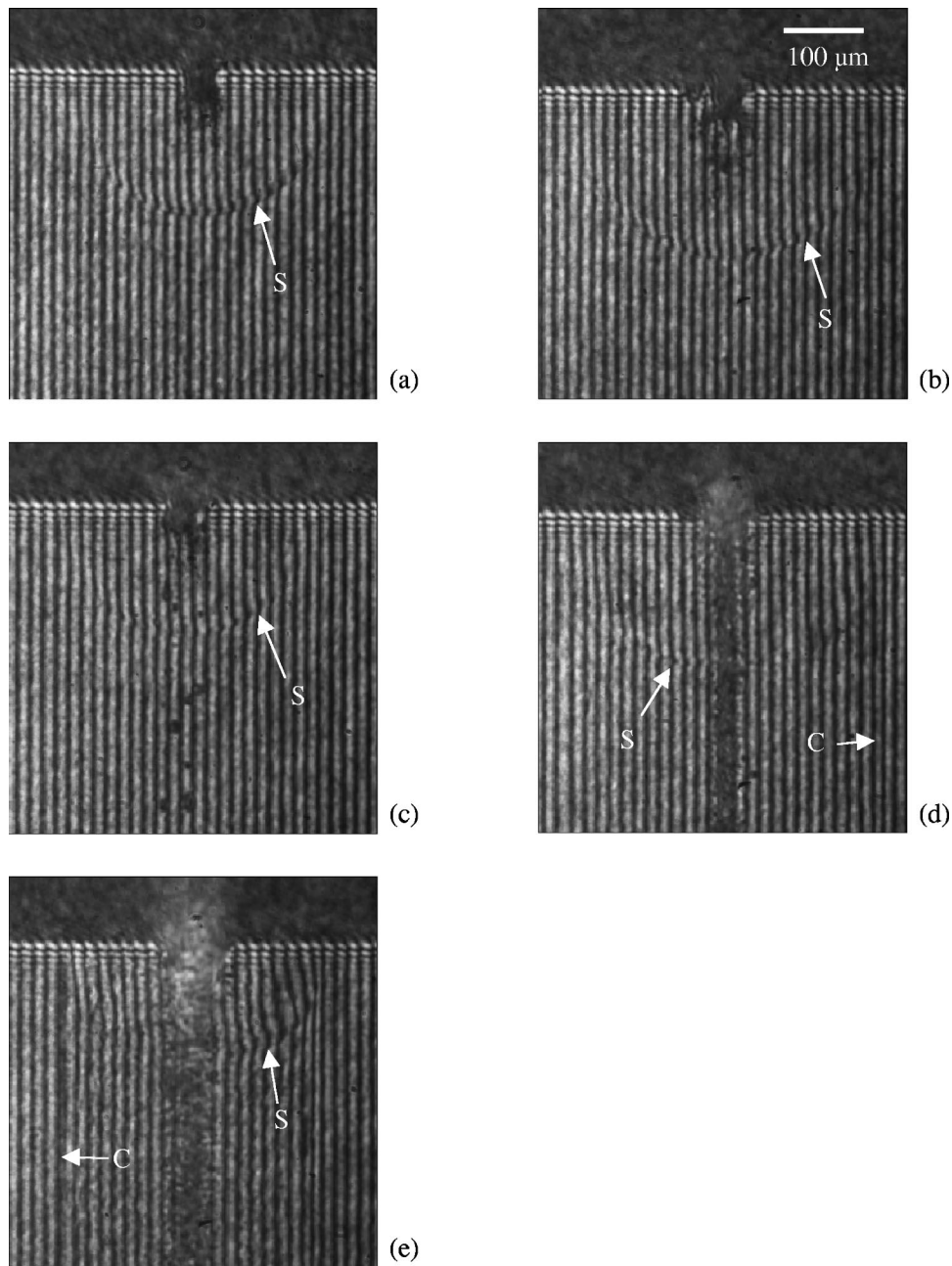


Fig. 8 Interferograms of the USLP-induced shock waves. The pulse durations are: (a) 130 fs, (b) 500 fs, (c) 1 ps, (d) 5 ps, and (e) 10 ps. Cylindrical waves from beam axis are observed from the images of 5 and 10 ps (S: spherical wave, C: cylindrical wave).

surface while vertical channel and cylindrical waves are also observed for 5–10 ps pulses. This result is consistent with the transition in our hard tissue studies; a possible explanation is given below.

The free electron number density (n) evolution during USLP irradiation can be described by²

$$\frac{\partial n}{\partial t} = \alpha I(t)n + P(I), \quad (1)$$

where α is a avalanche constant ($\text{cm}^2/\text{ps GW}$), $I(t)$ is the

beam intensity (GW/cm^2), and $P(I)$ is the multiphoton ionization rate. $P(I)$ is normally expressed as a function of I^k where

$$k = \text{integer} \left[\frac{E_g}{\hbar \omega} + 1 \right]$$

indicates how many photons are needed to cross band-gap energy E_g , where \hbar is the Plank's constant and ω is the light frequency. For example, for 1053 nm light in fused silica, k is 8. In case of water ablation by 800 nm light, $P(I)$ is propor-

tional to I^5 since the water band-gap energy is approximately 6.5 eV.²¹ Free electrons are generated not only by the linear term ($\alpha I n$, electron avalanche ionization) but also by the strong nonlinear term [$P(I)$, multiphoton ionization]. For development of avalanche ionization, initial “seed” electrons are needed. Such seed electrons are produced by multiphoton ionization when the laser intensity is high. For extremely short pulses (such as a few tens of femtoseconds) with high intensity, multiphoton ionization alone can produce enough electrons for material damage.^{1,22,23} For longer pulses, most electrons are produced by avalanche, nevertheless, multiphoton ionization plays an important role by creating necessary “seed” electrons. Detailed theoretical studies of electron evolution for water were reported by Noack and Vogel.¹

For plasma-mediated optical breakdown of material, the ablation threshold is usually defined as the fluence at which the free electron density (n) reaches the critical electron density ($n_{cr} \sim 10^{21}/\lambda^2 \text{ cm}^{-3}$ where λ is in μm). Above threshold, the critical electron density is reached within the duration of the pulse. When $n > n_{cr}$ the light penetrates approximately one skin depth into the plasma layer and is partially reflected. All energy deposition is confined to this surface plasma layer. For extremely short pulses where multiphoton ionization contributes significantly, n_c is reached near the pulse peak and the later half of the pulse is absorbed. However, when n is below n_{cr} the laser can penetrate into and through the plasma layer and deposit energy at depth. As the pulse duration lengthens, a supercritical plasma layer may be created only toward the end of the pulse. In this case the leading edge of the pulse is able to penetrate significantly into the material and deposit energy volumetrically [See Figures 8(d) and 8(e)]. This volumetrically deposited energy may not be useful for ablation since much of the material is not heated enough to vaporize it due to low deposited energy, although it may be melted or otherwise damaged. It was demonstrated that the free electrons are formed more rapidly for shorter pulses.¹ This implies that a larger fraction of the pulse energy is transmitted into the samples when longer pulses irradiate the material. It was also shown that more energy is needed to initiate the ablation of the material when using the longer pulses (Figures 3 and 7). Therefore, for longer pulses more energy is transmitted through the material causing distributed energy deposition. Energy deposition along the beam path will induce cylindrical waves as shown in this study.

In the case of hard tissue experiments, part of the pulse is transmitted through the surface and deposits energy in a similar way but over a shorter distance due to higher linear absorption. The deposited energy is too low to ablate the material but large enough to produce melting and change the crater morphology.

Interestingly, the hard and soft tissue experiments agree on the pulse duration corresponding to the transition of ablation patterns. Both results indicate that the transition occurs between 1 and 5 ps. The large transmission of the pulse energy for 5 ps pulses is indicated by the formation of the vertical channel during water ablation and this might explain why more thermal damage is observed for the hard tissue ablation. It is still not clear what this transition might mean in clinical applications. However, it is clear that tens of picosecond pulses will induce more thermal damage to the periphery of the target tissue. 1 ps pulses might be preferred if the manu-

facturing cost can be reduced using 1 ps pulse lasers rather than 100 fs lasers.

5 Conclusion

Ablation threshold and crater morphology studies show that 1 ps pulse duration might be suitable for low-damage and effective tissue ablation. Longer duration pulses waste more energy on collateral heating and mechanical damage.

Acknowledgments

This work was performed under the auspices of the U.S. Department of Energy at Lawrence Livermore National Laboratory under Contract No. W-7405-ENG-48.

References

1. J. Noack and A. Vogel, “Laser-induced plasma formation in water at nanosecond to femtosecond time scales: calculation of thresholds, absorption coefficients, and energy density,” *IEEE J. Quantum Electron.* **35**(8), 1156–1167 (1999).
2. B. C. Stuart, M. D. Feit, S. Herman, A. M. Rubenchik, B. W. Shore, and M. D. Perry, “Nanosecond-to-femtosecond laser-induced breakdown in dielectrics,” *Phys. Rev. B* **53**(4), 1749–1761 (1996).
3. A. A. Oraevsky, L. B. Da Silva, A. M. Rubenchik, M. D. Feit, M. E. Glinesky, M. D. Perry, B. M. Mammini, W. Small IV, and B. C. Stuart, “Plasma mediated ablation of biological tissues with nanosecond-to-femtosecond laser pulses: relative role of linear and nonlinear absorption,” *IEEE J. Sel. Top. Quantum Electron.* **2**(4), 801–809 (1996).
4. L. B. Da Silva et al., “Comparison of soft and hard tissue ablation with sub-ps and ns pulse lasers,” *Proc. SPIE* **2681**, 196–200 (1996).
5. J. Neev, L. B. Da Silva, M. D. Feit, M. D. Perry, A. M. Rubenchik, and B. C. Stuart, “Ultrashort pulse lasers for hard tissue ablation,” *IEEE J. Sel. Top. Quantum Electron.* **2**(4), 790–800 (1996).
6. M. Lenzner, J. Krüger, S. Sartania, Z. Cheng, Ch. Spielmann, G. Mourou, K. Kautek, and F. Krausz, “Femtosecond optical breakdown in dielectrics,” *Phys. Rev. Lett.* **80**(18), 4076–4079 (1998).
7. M. H. Niemz, “Threshold dependence of laser-induced optical breakdown on pulse duration,” *Appl. Phys. Lett.* **66**(10), 1181–1183 (1995).
8. F. H. Loesel, M. H. Niemz, J. F. Bille, and T. Juhasz, “Laser-induced optical breakdown on hard and soft tissues and its dependence on the pulse duration: experiment and model,” *IEEE J. Quantum Electron.* **32**, 1717–1722 (1996).
9. G. B. Altshuler, N. R. Belashenkov, V. B. Karasev, A. V. Skripnik, and A. A. Solounin, “Applications of ultrashort laser pulses in dentistry,” *Proc. SPIE* **2080**, 77–81 (1993).
10. A. M. Rubenchik, L. B. Da Silva, M. D. Feit, S. Lane, R. London, M. D. Perry, and B. C. Stuart, “Dental tissue processing with ultra-short pulse laser,” *Proc. SPIE* **2672**, 222–230 (1996).
11. A. Vogel, M. R. C. Capon, M. N. Asiyov-Vogel, and R. Birngruber, “Intraocular photodisruption with picosecond and nanosecond laser pulses: tissue effects in cornea, lens, and retina,” *Invest. Ophthalmol. Visual Sci.* **35**(7), 3032–3044 (1994).
12. A. Vogel, T. Günther, M. Asiyov-Vogel, and R. Birngruber, “Factors determining the refractive effects of intrastromal photorefractive keratectomy with the picosecond laser,” *J. Cataract Refractive Surg.* **23**, 1301–1310 (1997).
13. T. Juhasz, G. A. Kastis, C. Suárez, Z. Bor, and W. E. Bron, “Time-resolved observations of shock waves and cavitation bubbles generated by femtosecond laser pulses in corneal tissue and water,” *Lasers Surg. Med.* **19**, 23–31 (1996).
14. X.-H. Hu and T. Juhasz, “Study of corneal ablation with picosecond laser pulses at 211 nm and 263 nm,” *Lasers Surg. Med.* **18**, 373–380 (1996).
15. B.-M. Kim, M. D. Feit, A. M. Rubenchik, B. M. Mammini, and L. B. Da Silva, “Optical feedback signal for ultrashort laser pulse ablation of tissue,” *Appl. Surf. Sci.* **127–129**, 857–862 (1998).
16. E. N. Glezer, C. B. Schaffer, N. Nishimura, and E. Mazur, “Minimally disruptive laser-induced breakdown in water,” *Opt. Lett.* **22**, 1817–1819 (1997).
17. J. Noack and A. Vogel, “Single-shot spatially resolved characteriza-

- tion of laser-induced shock waves in water," *Appl. Opt.* **37**, 4092–4099 (1998).
18. A. Vogel, S. Busch, and U. Parlitz, "Shock wave emission and cavitation bubble generation by picosecond and nanosecond optical breakdown in water," *J. Acoust. Soc. Am.* **100**, 148–165 (1996).
 19. F. H. Loesel, J. P. Fischer, M. H. Goetz, C. Horvath, T. Juhasz, F. Noack, N. Suhm, and J. F. Bille, "Non-thermal ablation of neural tissue with femtosecond laser pulses," *Appl. Phys. B: Lasers Opt.* **66**(1), 121–128 (1998).
 20. B. Majaron and M. Lukac, "Calculation of crater shape in pulsed laser ablation of hard tissues," *Lasers Surg. Med.* **24**, 55–60 (1999).
 21. F. Williams, S. P. Varma, and S. Hillenius, "Liquid water as a lone-pair amorphous semiconductor," *J. Chem. Phys.* **64**, 1549–1554 (1976).
 22. Q. Feng, J. V. Moloney, A. C. Newell, E. M. Wright, K. Cook, P. K. Kennedy, D. X. Hammer, B. A. Rockwell, and B. A. Rockwell, "Theory and simulation on the threshold of water breakdown induced by focused ultrashort laser pulses," *IEEE J. Quantum Electron.* **33**, 127–137 (1997).
 23. B. C. Stuart, M. D. Feit, S. Herman, A. M. Rubehcnik, B. W. Shore, and M. D. Perry, "Optical ablation by high-power short-pulse lasers," *J. Opt. Soc. Am. B* **13**, 459–468 (1996).